

Unleashing the Temporal Potential of Stereo Event Cameras for Continuous-Time 3D Object Detection

Jae-Young Kang*, Hoonhee Cho*, and Kuk-Jin Yoon
KAIST

{mickeykang, gnsgnsgml, kjyoon}@kaist.ac.kr

Abstract

3D object detection is essential for autonomous systems, enabling precise localization and dimension estimation. While LiDAR and RGB cameras are widely used, their fixed frame rates create perception gaps in high-speed scenarios. Event cameras, with their asynchronous nature and high temporal resolution, offer a solution by capturing motion continuously. The recent approach, which integrates event cameras with conventional sensors for continuous-time detection, struggles in fast-motion scenarios due to its dependency on synchronized sensors. We propose a novel stereo 3D object detection framework that relies solely on event cameras, eliminating the need for conventional 3D sensors. To compensate for the lack of semantic and geometric information in event data, we introduce a dual filter mechanism that extracts both. Additionally, we enhance regression by aligning bounding boxes with object-centric information. Experiments show that our method outperforms prior approaches in dynamic environments, demonstrating the potential of event cameras for robust, continuous-time 3D perception. The code is available at <https://github.com/mickeykang16/Ev-Stereo3D>.

1. Introduction

3D object detection is essential for accurately identifying the position and dimensions of surrounding objects, making it a fundamental task in autonomous systems. Multi-modal sensors, such as LiDAR and RGB cameras, play a key role. However, fixed-frame rate sensors have discrete intervals during which data cannot be collected, resulting in inevitable detection delays. This delay in capturing dynamic changes can significantly impact real-time decision-making, emphasizing the importance of high temporal resolution for reliable autonomous driving.

Event cameras [27] are asynchronous sensors that continuously stream data over time, allowing them to break the trade-off between bandwidth and delay. Their high tem-

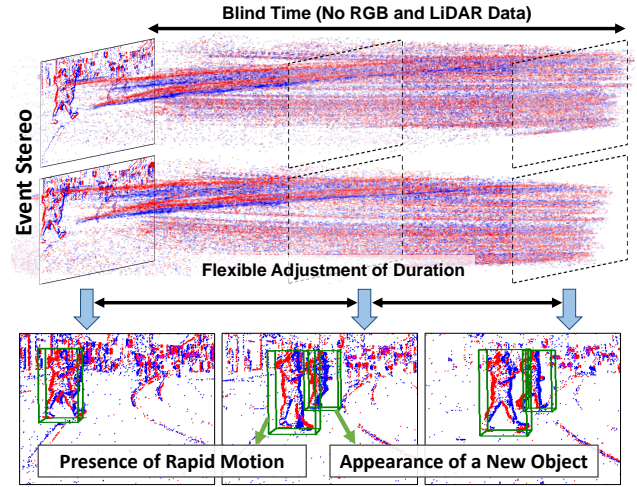


Figure 1. During blind time, our method enables fast and large motion-aware continuous 3D object detection at arbitrary points in time, including for newly appearing objects.

poral resolution makes them well-suited for capturing fast motion, enabling high-speed perception even in dynamic scenarios. This capability is particularly beneficial for autonomous driving, where rapid response is critical for accident prevention and safe navigation.

A recent work, Ev-3DOD [22], integrates an RGB camera, LiDAR, and an event camera to overcome the frame-rate limitations of conventional sensors in 3D object detection. By incorporating event data, it enables perception even during periods when LiDAR and RGB cameras are unavailable. Notably, it introduces continuous-time 3D object detection, allowing inference at arbitrary timestamps before the next synchronized sensor data arrives. Continuous-time 3D object detection enables accurate inference beyond the timeframes when synchronized sensors, such as RGB and LiDAR, provide data. Ev-3DOD [22] defined periods with LiDAR and RGB data as active time and intervals without them as blind time, demonstrating that event cameras can facilitate 3D detection during these blind periods.

However, approaches that temporally propagate LiDAR-

*Equal contribution.

and image-based detection with events are highly dependent on synchronized sensors introducing limitations in dynamic environments. For example, in scenarios like drones with rapid motion during adjacent active times, or high-speed driving causing significant movement during blind periods, fixed frame-rate sensor data does not fully reflect the current 3D geometry. As a result, errors are accumulated over blind time, leading to frequent detection failures.

To this end, we propose an event stereo setup that performs precise 3D object detection using only sparse and asynchronous event cameras to address the limitations of conventional sensors. As shown in Fig. 1, event stereo can compute 3D information even during blind time, enabling the detection of large-moving and newly appearing objects, which are scenarios that synchronized sensors cannot handle in blind time.

One of the challenges when using only event data for 3D object detection is its sparse nature. Event data lacks both semantic and geometric information compared to images and LiDAR, making accurate classification and regression particularly difficult. To overcome this, we propose a dual semantic-geometric filter module that collaboratively filters and enhances both information, fully leveraging stereo event data. The event semantic feature filters the geometric depth feature while the geometric feature simultaneously enhances the semantic information through the estimated disparity. Additionally, following the global detection head, a dense, object-centric semantic event feature is employed to align the local 3D offsets of the bounding boxes, thereby enhancing regression performance.

Our proposed method achieves comparable performance in continuous-time 3D object detection without relying on rich fixed frame-rate sensor data. Specifically, through experiments in which the scene undergoes significant changes due to large motion within the same duration, as well as tests involving various intervals for inference, our approach outperforms existing methods. This result can be attributed to the use of asynchronous sensors, which offer distinct advantages in handling dynamic scenarios while fully utilizing both semantic and geometric information of events. The paper highlights the potential and scalability of event cameras to enhance 3D object detection in various environments.

2. Related Works

Camera-based 3D Object Detection. Cameras offer significant cost advantages over LiDAR, leading many researchers to focus on developing methods for 3D object detection using image-only inputs [15, 40, 44, 57, 60, 62, 66, 87, 91, 92]. However, image-based 3D detection faces challenges due to the lack of direct depth information. To address this, several works [11, 12, 34, 49, 61] propose using stereo and multi-camera systems to compute 3D geometry through multiple views. Despite these advancements, accu-

rately estimating depth from images remains challenging, causing image-based methods to underperform compared to LiDAR-based approaches.

LiDAR-based 3D Object Detection. LiDAR-based 3D object detection can reliably estimate 3D bounding boxes using point clouds captured from LiDAR sensors.

Research on representing 3D information from LiDAR has been conducted through various approaches, including point-based methods [25, 39, 82, 84, 99, 102, 108], voxel-based methods [24, 33, 38, 38, 46, 52, 67, 81, 93, 96, 104], and point-voxel fusion networks [37, 68, 83, 98].

To further boost the performance of LiDAR-based 3D detection, multi-modal sensor fusion [9, 41, 42, 50, 51, 59, 86, 94, 103] has emerged, where different sensors, such as cameras and LiDAR, complement each other. Fusion approaches are categorized into early [16, 89, 97], middle [54–56, 58, 63, 76, 78, 100], and late fusion [2, 50, 71]. Multi-modal 3D object detection has garnered significant attention for its ability to improve accuracy and enhance performance compared to unimodal methods. However, there is still room for improvement in terms of safety in autonomous driving. LiDAR and cameras have limited time resolution (*i.e.*, 10-20 Hz) because of their relatively high bandwidths. These limitations are especially noticeable in scenarios like high-speed driving or drone flight. To improve safety, algorithms that can operate at higher speeds are crucial.

Event-based Stereo. Event cameras are well-suited for capturing dynamic scenes due to their high temporal resolution, low latency, and ability to operate effectively in challenging lighting conditions. Based on these characteristics, approaches using event cameras in a stereo setup [1, 19–21, 69, 70, 106, 109, 112] have been proposed to better understand the surrounding 3D dynamic scenes. Additionally, research has explored using event cameras in a stereo setup alongside other sensors [3, 10, 17, 18, 65, 107], aiming to leverage the strengths of both event data and conventional sensors to enhance perception capabilities. Building on this research direction, we demonstrate that 3D object detection can be performed using only asynchronous event cameras. Furthermore, we highlight the potential of event cameras for 3D detection in dynamic and rapid motion scenarios.

Event-based Object Detection. On the 2D image plane, numerous studies [6, 28, 30, 36, 43, 47, 48, 53, 72, 73, 75, 90, 113] have leveraged the event camera’s sensitivity to moving objects for object detection. Various architectures, including graph-based [5, 29, 79], spiking [101], and sparse [74] neural networks, have been explored to achieve streamlined and compelling results tailored to specific objectives. A recent study [22] demonstrated the advantages of high temporal resolution of event cameras in 3D object detection by integrating them with LiDAR and RGB cameras. This study addressed the limitation of synchronized sensors, such as RGB cameras and LiDAR, which operate

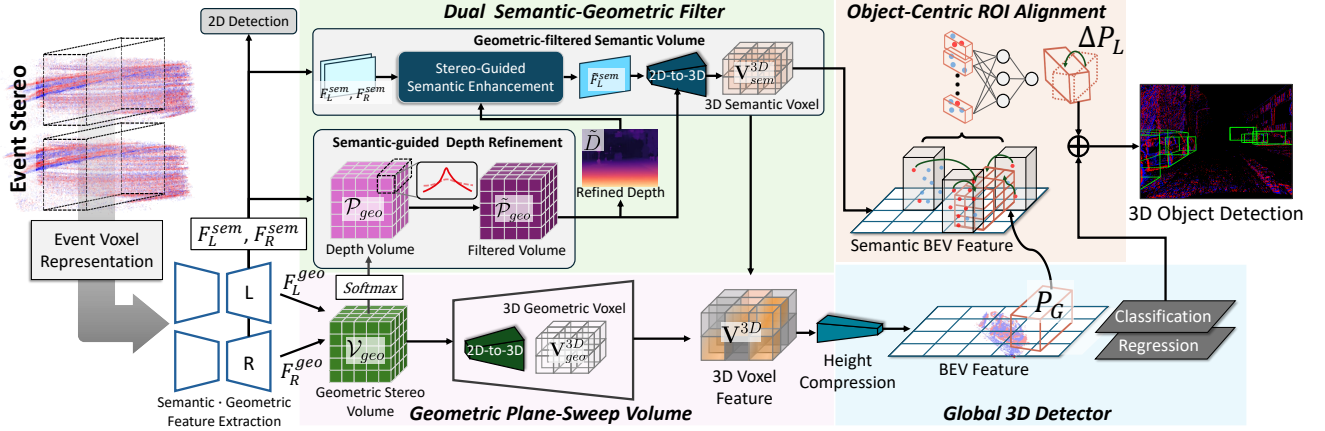


Figure 2. Overview of the proposed method. Our method is categorized into four components: Geometric Plane-Sweep Volume (Sec. 3.2), Dual Semantic-Geometric Filter (Sec. 3.3), Global 3D Detector (Sec. 3.4), and Object-Centric ROI Alignment (Sec. 3.5).

at fixed frame rates and restrict inference to discrete time intervals. By integrating event cameras, the proposed approach overcomes this constraint, enabling continuous 3D detection even in the absence of synchronized sensor input.

Despite these promising results, the approach remains partially dependent on synchronization, as critical information is solely derived from RGB and LiDAR. Consequently, significant errors may occur when rapid motion leads to substantial scene changes during blind time. To address this limitation, we propose the first fully asynchronous system for 3D object detection, utilizing a stereo event camera setup. Thanks to this asynchronous advantage, our method maintains strong performance even when the scene undergoes significant changes during the blind time or when inference is required at a finer continuous-time scale.

3. Methods

3.1. Preliminaries

Event Camera. Traditional frame-based cameras capture images at fixed intervals, whereas event cameras operate asynchronously, recording changes in logarithmic intensity $L(u, v, t)$ only when they exceed a predefined threshold \mathcal{C} . This can be expressed as:

$$L(u, v, t) - L(u, v, t - \Delta t) \geq \mathbf{p}\mathcal{C}, \quad \mathbf{p} \in \{-1, +1\}, \quad (1)$$

where Δt represents the time difference, and \mathbf{p} denotes event polarity, indicating either negative or positive events. The event stream \mathcal{E} consists of events e_i with spatial coordinates (u_i, v_i) , timestamp t_i , and polarity p_i :

$$\mathcal{E} = \{e_i\}_{i=1}^N, \quad e_i = (u_i, v_i, t_i, p_i). \quad (2)$$

Event Representation. We adopt a voxel grid [111] representation, where events are discretized along the time axis into B bins. Given N input events, timestamps are normalized to $[0, B - 1]$, and the event volume is constructed as:

$$E(u, v, b) = \sum_{i=1}^N p_i k_B(u - u_i) k_B(v - v_i) k_B(b - b_i^*), \quad (3)$$

where $b_i^* = (B - 1)(t_i - t_1)/(t_N - t_1)$ and $k_B(a)$ is a bilinear sampling kernel. The voxel grid allows efficient feature extraction via 2D convolution across spatial dimensions while conserving temporal information.

We use the event stream from the recent interval $\Delta\tau$, denoted as $\mathcal{E}_{(\tau-\Delta\tau) \rightarrow \tau} = \{(u, v, t, p) \mid \tau - \Delta\tau \leq t < \tau\}$, to detect 3D boxes at time τ . To achieve the continuous-time detection framework, $\Delta\tau$ can adapt flexibly to different scenarios. This enables detection at arbitrary time points, making the framework adaptable to various situations. To simplify notation in this section, we represent the voxel grids generated from $\mathcal{E}_{(\tau-\Delta\tau) \rightarrow \tau}$ as E_L and E_R for the left and right cameras, respectively.

3.2. Geometric Plane-Sweep Volume

We illustrate the overall training pipeline in Fig. 2. We modify the PSMNet [7] to design our feature extractor and incorporated an additional feature head to disentangle the roles of semantics-based detection and geometric scene construction. This allows the extractor to separately extract semantic features $F_{L,R}^{sem}$ and geometric features $F_{L,R}^{geo}$, each with a dimension of $\mathbb{R}^{H \times W \times C}$. The semantic feature activates well on objects through an auxiliary 2D dense head on the 2D image. The geometric feature activates across the entire scene on the stereo images, concentrating on finding correspondences. First, we generate a geometric plane-sweep volume $\mathcal{V}_{geo} \in \mathbb{R}^{H \times W \times D \times C}$ by concatenating left and corresponding right geometric features at each depth level D , as done in previous works [11, 34]. The volume is defined as:

$$\mathcal{V}_{geo}(u, v, w) = (F_L^{geo}(u, v) || F_R^{geo}(u - \frac{fL}{d(w)}, v)), \quad (4)$$

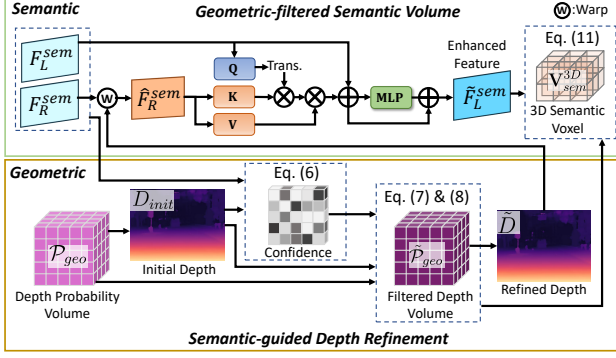


Figure 3. Dual semantic-geometric filter. Semantic and geometric information interact complementarily to enhance both the semantic features and the depth volume.

where (u, v) are pixel coordinates, \parallel denotes the concatenation, $w = 0, 1, \dots$ is the candidate depth index, and $d(w) = w \cdot v_d + z_{\min}$ is the function to calculate the corresponding depth, where v_d is the depth interval and z_{\min} is the minimum depth of the detection area. f and L represent the camera focal length and the baseline of the stereo camera pair, respectively. From the geometric stereo volume \mathcal{V}_{geo} , we apply 3D convolutions to reduce the channel dimension, followed by a softmax operation along the depth dimension, resulting in a depth probability volume $\mathcal{P}_{geo} \in \mathbb{R}^{H \times W \times D}$, where $\mathcal{P}_{geo}(u, v, :)$ represents the depth probability for pixel (u, v) across all depth levels.

To transform the feature volume from stereo space to a 3D space, the 3D detection area is segmented into uniformly sized voxels, resulting in $\mathbf{V}_{geo}^{3D} \in \mathbb{R}^{X \times Y \times Z \times C}$. For each voxel, its center coordinates (x, y, z) are projected back into the stereo space using the intrinsic parameters K , resulting in the reprojected pixel coordinates (u, v) and a corresponding depth index $d^{-1}(z) = (z - z_{\min})/v_d$ as:

$$\mathbf{V}_{geo}^{3D}(x, y, z) = \mathcal{V}_{geo}(u, v, d^{-1}(z)). \quad (5)$$

3.3. Dual Semantic-Geometric Filter

Along with the geometric volume, we leverage the event camera’s robustness in detecting objects on the 2D plane by using semantic features to construct a 3D semantic volume $\mathbf{V}_{sem}^{3D} \in \mathbb{R}^{X \times Y \times Z \times C}$. Creating a 3D volume with only semantic features fails to capture geometric properties. To address this, we propose a dual semantic-geometric filter that combines both semantic and geometric information, as shown in Figure 3.

Semantic-guided Depth Refinement. One of the key challenges in 3D detection using stereo cameras is achieving accurate depth inference. Unlike LiDAR, stereo cameras do not provide direct depth measurements from the sensor. To enhance depth accuracy, we utilize semantic information to refine the geometric cost volume. As shown in Fig. 3, we first estimate the initial depth D_{init} by computing the

weighted sum over all depth levels using the depth probability volume \mathcal{P}_{geo} . Additionally, to refine the depth distribution volume by transferring accuracy through the semantic feature, which effectively captures semantic information about the scene, we compute the similarity for each pixel based on the predicted depth as:

$$S(u, v) = \langle F_L^{sem}(u, v), F_R^{sem}(u - \frac{fL}{D_{init}(u, v)}, v) \rangle, \quad (6)$$

where $\langle \cdot, \cdot \rangle$ denotes the inner product for similarity. Similar to previous works [8, 77, 80, 95] that handle confidence in stereo matching, we also compute confidence as follows:

$$C(u, v) = \sum_w \mathcal{P}_{geo}(u, v, w) \cdot (d(w) - D_{init}(u, v))^2, \quad (7)$$

We aim to refine the depth distribution by considering both stereo similarity and confidence. Adapting the refinement process from [95], we generate filtered volume, $\tilde{\mathcal{P}}_{geo}$, by incorporating neighboring probabilities as follows:

$$W_m(u, v) = S_m(u, v) \cdot \text{sigmoid}(C_m(u, v)),$$

$$\tilde{\mathcal{P}}_{geo}(u, v, w) = \sum_{m=1}^M \mathcal{P}_{geo}(u, v, w) \cdot \text{softmax}_m(W_m(u, v)), \quad (8)$$

where $m = 1, 2, 3, \dots, M$ are the sampled neighboring pixels and softmax_m denotes a softmax across the m dimension. Through this refinement process, depth ambiguity can be resolved, and we estimate the refined depth, \tilde{D} , from the refined probability.

Geometric-filtered Semantic Volume. Although semantic features are well activated for objects, event data is sparse along the spatial dimension, often leading to ambiguity. To compensate for this lack of information, we enhance the left features using the estimated depth and the semantic features from the right camera. As shown in the bottom of Fig. 3, we warp the right semantic features to the left camera using the estimated depth: $\hat{F}_R^{sem} = \text{Warp}(F_R^{sem}, \tilde{D})$. However, directly using these warped features may introduce occlusion issues and fail to fully address potential misalignments between stereo cameras. To handle these challenges, we apply a transformer-based channel attention mechanism to generate enhanced semantic features. We generate the query, key, and value features as follows: $\mathbf{Q} = W_Q(F_L^{sem})$, $\mathbf{K} = W_K(\hat{F}_R^{sem})$, and $\mathbf{V} = W_V(\hat{F}_R^{sem})$, where $W_{(\cdot)}$ represents a 1×1 convolution. The results of the transformer are computed in this manner:

$$\mathbb{A}(F_L^{sem}, \hat{F}_R^{sem}) = F_L^{sem} + W_{\mathbb{A}}(\text{softmax}(\frac{\mathbf{Q}\mathbf{K}^T}{\alpha}) \cdot \mathbf{V}) \quad (9)$$

where α is a learnable parameter. Finally, the geometrically enhanced semantic feature \tilde{F}_L^{sem} is obtained:

$$\tilde{F}_L^{sem} = F_L^{sem} + \text{MLP}(\mathbb{A}) + \mathbb{A}. \quad (10)$$

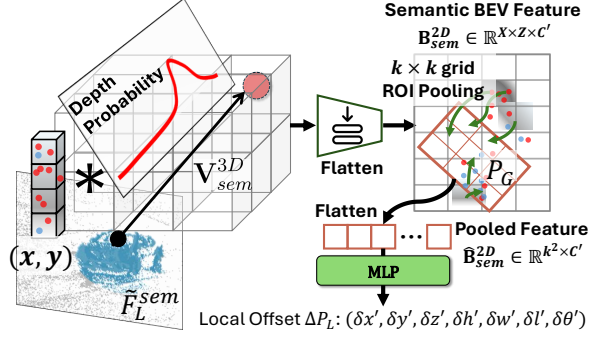


Figure 4. Illustration of the object-centric ROI alignment.

Similar to Eq. (5), voxels can be projected onto the image plane to map 2D semantic features to 3D. However, to ensure the transformation is based on geometric information, we apply a depth probability mask as:

$$\mathbf{V}_{sem}^{3D}(x, y, z) = \tilde{F}_L^{sem}(u, v) \cdot \tilde{P}_{geo}(u, v, d^{-1}(z)) \quad (11)$$

Fusion of Semantic and Geometric Voxels. We generate two types of voxels in the 3D space: one specialized for geometric information, \mathbf{V}_{geo}^{3D} , and the other for semantic information, \mathbf{V}_{sem}^{3D} . To integrate the two voxels into a unified 3D voxel that effectively combines both aspects, we concatenate and then merged them through 3D convolution, resulting in the fused voxel, \mathbf{V}^{3D} .

3.4. Global 3D Detector

Inspired by recent stereo 3D detection approaches [11, 12, 34], we designed an anchor-based detector. The bird’s-eye view (BEV) feature strikes a balance between accuracy and computational efficiency in 3D detection for autonomous driving. The unified 3D voxel features $\mathbf{V}^{3D} \in \mathbb{R}^{X \times Y \times Z \times C}$ are downsampled along the height dimension to produce a BEV feature of size (X, Z) . We utilize fixed-size class anchors, determined based on the training set statistics, and assign a predefined number of anchors with varying sizes and orientations to each BEV feature location (x, z) . Similar to previous works [11, 12, 34], the dense head network performs a regression from the anchor $A = (x_a, y_a, z_a, h_a, w_a, l_a, \theta_a)$ to predict the offset $\Delta P_G = (\delta x, \delta y, \delta z, \delta h, \delta w, \delta l, \delta \theta)$. The final prediction is calculated by applying an offset to the anchor to determine the global position using the box decoding function g_d ,

$$P_G = g_d(A, \Delta P_G) = (x_a + \delta x, y_a + \delta y, z_a + \delta z, h_a e^{\delta h}, w_a e^{\delta w}, l_a e^{\delta l}, \theta_a + \frac{\pi}{2} \tanh(\delta \theta)). \quad (12)$$

3.5. Object-Centric ROI Alignment

The geometric-semantic fused 3D voxels, \mathbf{V}^{3D} , generated through the semantic-geometric dual filter contain accurate

depth and rich semantic information, enabling bounding box prediction in the global scene. However, a single-stage global regression can struggle with ambiguity caused by the motion of objects and the movement of the ego vehicle, especially as motion intensifies, necessitating a method that aligns more accurately with the object. To this end, we propose a method for locally aligning the ROI around the object’s bounding box.

ROI Pooling and Local Regression. As shown in Fig. 4, we use the semantic voxel, \mathbf{V}_{sem}^{3D} , which focuses on the object and provides rich edge information from event-based semantic data, making it advantageous for ROI alignment. To optimize the computation of alignment, and because most stereo-based detections are prone to error along the X and Z dimensions, we project the voxel features onto the BEV, which corresponds to the transformation of $\mathbf{B}_{sem}^{2D} \in \mathbb{R}^{X \times Z \times C'}$ to the BEV of \mathbf{V}_{sem}^{3D} , rather than using them directly. Since \mathbf{B}_{sem}^{2D} is splatted based on depth probabilities, it tends to cluster around the high-likelihood hypotheses of the predicted boxes. Therefore, to ensure that not only the exactly overlapping features but also the surrounding information is aggregated during alignment, we use a pooling scheme. Specifically, each bounding box prediction from global 3D detector, P_G , is split into an $k \times k$ voxel grid. The semantic BEV feature, \mathbf{B}_{sem}^{2D} , is then pooled [23] for each voxel grid. The pooled feature of each bounding box, $\hat{\mathbf{B}}_{sem}^{2D} \in \mathbb{R}^{k^2 \times C'}$, encodes object-centric local information, serving as a cue for precisely aligning the box. Each pooled feature passes through an MLP layer to predict the local alignment offset, $\Delta P_L = (\delta x', \delta y', \delta z', \delta h', \delta w', \delta l', \delta \theta')$. The final fine-grained regression, \tilde{P}_G , is calculated by box decoding function: $\tilde{P}_G = g_d(P_G, \Delta P_L)$

3.6. Objective Function

A multi-task loss was applied to train the network, which includes the geometric plane-sweep volume, the dual semantic-geometric branch, the global 3D detector head, and object-centric ROI alignment module as follows:

$$\mathcal{L} = \mathcal{L}_{depth}^{init} + \mathcal{L}_{depth}^{refine} + \mathcal{L}_{2D} + \mathcal{L}_{cls} + \mathcal{L}_{reg}^{global} + \mathcal{L}_{reg}^{local}. \quad (13)$$

where $\mathcal{L}_{depth}^{init}$, \mathcal{L}_{2D} , \mathcal{L}_{cls} are adapted from uni-modal depth loss, 2D detection loss, and classification loss in [34]. For refined depth loss, we utilized *smooth* L_1 loss [45] as

$$\mathcal{L}_{depth}^{refine} = \text{smooth}_{L_1}(D_{gt} - \tilde{D}). \quad (14)$$

The regression loss for the global 3D detector and object-centric ROI alignment are as follows:

$$\mathcal{L}_{reg}^{global} = \mathcal{L}_{reg}(P_G, G), \quad \mathcal{L}_{reg}^{local} = \mathcal{L}_{reg}(\tilde{P}_G, G) \quad (15)$$

where G refers to 3D ground-truth bounding box and \mathcal{L}_{reg} is 3D regression loss adapted from [34].

Table 1. Comparison on the DSEC-3DOD dataset for vehicle (IoU = 0.7) and pedestrian (IoU = 0.5) detection on 3D and BEV. We follow the evaluation protocol of Ev-3DOD [22] for 100 FPS 3D detection in blind time. Mod. is an abbreviation for moderate, and easy and moderate represent difficulty levels. VEH and PED represent vehicle and pedestrian, respectively.

Modality	Methods	VEH AP _{3D}		VEH AP _{BEV}		PED AP _{3D}		PED AP _{BEV}	
		Easy	Mod.	Easy	Mod.	Easy	Mod.	Easy	Mod.
LiDAR	VoxelNeXt [14]	12.66	11.06	31.46	28.39	10.59	6.61	12.77	7.96
	HEDNet [105]	14.31	12.96	29.94	27.85	10.16	8.29	11.90	6.89
LiDAR+RGB	Focals Conv [13]	12.71	11.69	26.14	23.83	8.92	5.50	12.54	7.83
	LoGoNet [50]	17.65	15.39	32.55	29.19	11.66	8.20	15.09	9.77
LiDAR+RGB+Event	Ev-3DOD [22]	29.53	25.07	49.31	44.44	<u>18.42</u>	<u>12.49</u>	29.06	20.34
RGB-Stereo	DSGN [11]	16.29	13.45	31.90	27.53	4.06	2.42	6.08	3.74
	LIGA [34]	14.26	10.98	27.25	25.11	6.02	3.58	8.73	4.89
Event-Stereo	Ours	<u>23.47</u>	<u>19.62</u>	<u>40.13</u>	<u>33.03</u>	19.86	12.93	<u>22.91</u>	<u>14.34</u>

4. Experiments

4.1. Dataset

DSEC-3DOD Dataset. The DSEC-3DOD dataset is the real-world event-based 3D detection dataset introduced in the Ev-3DOD [22]. It is based on the DSEC [31], a stereo event dataset for driving scenarios. DSEC-3DOD contains manually created 10 FPS annotations for vehicle and pedestrian classes and provides blind-time annotations at 100 FPS through interpolation and refinement. We used the widely adopted KITTI metric [32] from frame-based stereo methods, which measures performance in both BEV (bird-eye-view) and 3D for each class.

4.2. Experiment Setup

3D Detection during Blind Time. Consistent with the training and evaluation protocol of existing event-based 3D object detection [22], we train and evaluate using 100 FPS annotations during blind time, when no LiDAR data is available due to the fixed frame rate of LiDAR (*i.e.*, 10 FPS). To achieve this, we sliced the event stream at $\Delta\tau = 10$ ms and converted it into a voxel grid.

Motion Scale and Time Slice. The strength of event cameras lies in their ability to provide continuous information over time, even in dynamic motion [4, 26]. Therefore, experiments on dynamic and long-range motion during blind time are crucial to demonstrate the advantages of the asynchronous setup. However, the DSEC-3DOD dataset mostly lacks such scenes, as its average ego velocity is below 10 m/s. To address this, we introduce an experimental setup, **motion scale** (MS), which scales time axis for large motion experiments that closely resemble the real world. Accumulation and normalization of events over a longer period can approximate events with larger motion over the same time span. Therefore, increasing the motion scale in experiments can depict dynamic environments by skipping consecutive annotations and accumulating events over a longer period. **Time slice** (TS) refers to the number of divisions applied

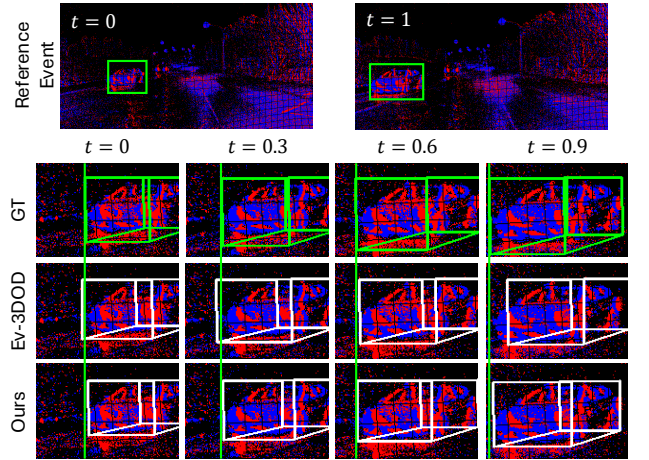


Figure 5. Comparison of 3D detection during blind time. $t = 0$ and $t = 1$ represent active time, while $t = 0.3, 0.6$, and 0.9 indicate normalized blind time intervals.

to the blind time, where detection performance is evaluated at each time slice instance. Since various event input durations are used, this setup reflects the real-world demand for asynchronous detection. The baseline setup is defined with a motion scale of 1 and a time slice of 10, which corresponds to the 10 FPS fixed-frame rate data provided in the DSEC-3DOD dataset and the blind time annotations sliced into 10 parts (*i.e.*, 100 FPS GT). To ensure compatibility with the original ground truth, experiments were conducted with motion scale values of 2 and 4 and time slice values of 10 and 20. The model is trained using the original 100 FPS GT with a motion scale of 1 and a time slice of 10 and is evaluated across various motion scales and time slices. More details about the experimental settings are provided in the supplementary material.

4.3. Results on 3D Detection during Blind Time

Table 1 provides the results of 3D detection performed during blind time. Results from previous works [13, 14, 50,

Table 2. Performance evaluation across various motion scales and time slices, presenting results for the easy difficulty level. Each entry corresponds to 3D / BEV detection results. VEH and PED represent vehicle and pedestrian, respectively.

Motion Scale	Time Slice	Class	LiDAR		LiDAR+RGB		LiDAR+RGB+Event	RGB Stereo		Event Stereo
			VoxelNeXt [14]	HEDNet [105]	Focals Conv [13]	LoGoNet [50]	Ev-3DOD [22]	DSGN [11]	LIGA [34]	Ours
$\times 2$	$\times 10$	VEH	5.05 / 13.00	6.03 / 12.87	5.95 / 12.48	5.97 / 13.57	<u>15.68</u> / <u>30.59</u>	7.33 / 17.36	6.00 / 12.87	22.72 / 39.81
		PED	4.07 / 4.89	3.40 / 4.05	3.16 / 4.79	2.24 / 3.72	<u>7.88</u> / <u>12.19</u>	1.87 / 3.04	2.27 / 4.00	19.04 / 22.71
	$\times 20$	VEH	4.34 / 11.76	5.26 / 11.67	5.76 / 11.40	5.42 / 12.40	<u>15.96</u> / <u>31.13</u>	7.13 / 16.43	5.67 / 12.00	23.47 / 40.13
		PED	<u>3.83</u> / <u>4.31</u>	2.60 / 3.49	2.66 / 3.86	1.91 / 2.90	1.47 / 2.63	1.84 / 2.99	2.08 / 3.01	19.86 / 22.91
$\times 4$	$\times 10$	VEH	2.05 / 5.22	2.87 / 4.63	2.73 / 4.48	1.90 / 5.26	<u>6.24</u> / <u>11.62</u>	3.12 / 7.20	2.10 / 4.89	20.70 / 37.08
		PED	2.21 / 2.44	1.64 / 1.85	1.34 / 1.85	1.17 / 1.55	<u>3.04</u> / <u>4.09</u>	0.60 / 0.77	1.11 / 1.30	16.71 / 21.93
	$\times 20$	VEH	1.71 / 4.55	2.27 / 4.29	2.73 / 3.94	1.90 / 4.66	<u>6.36</u> / <u>11.70</u>	3.09 / 6.52	1.54 / 4.17	22.72 / 39.81
		PED	<u>2.14</u> / <u>2.17</u>	1.10 / 1.42	1.02 / 1.44	0.53 / 1.28	0.39 / 0.43	0.59 / 0.75	0.82 / 1.12	19.04 / 22.71

[105] were taken from the supplementary material of Ev-3DOD [22], while we trained and evaluated frame-based stereo methods, DSGN [11] and LIGA [34], from scratch. Methods relying solely on synchronized sensors struggle to handle blind time, resulting in poor performance. On the other hand, both Ev-3DOD and our method utilize event cameras to overcome the limitations of fixed frame rates, enabling effective 3D detection during blind time and achieving high performance. While Ev-3DOD benefits from LiDAR-based depth information, generally outperforming our event-only approach, it is noteworthy that our method achieves superior performance in pedestrian AP_{3D} . Pedestrian detection requires fine detail, and our high performance on this class is due to specialized modules that effectively leverage semantic features from event data.

Figure 5 illustrates another advantage of the asynchronous setup. While Ev-3DOD shows a decline in qualitative results as it moves further from active time 0, where LiDAR data is available, our method maintains high performance by computing geometric information from events, allowing it to operate independently of active time.

4.4. Diverse Motion Scales and Time Slices

Table 2 shows the comparison of ours with different methods across various motion scales and time slices. Methods relying solely on synchronized sensors [11, 13, 14, 34, 50, 105] exhibit a significant performance drop as the motion scale increases during blind time. Our primary comparison method, Ev-3DOD [22], utilizes event data during blind time, allowing it to handle moderate scenarios well, as shown in Table 1. However, as the motion increases, its performance significantly drops. This is because Ev-3DOD relies entirely on LiDAR for 3D geometric information, and when large motion occurs, scene changes make past geometric information less useful for the present. In contrast, our method computes 3D geometric information using asynchronous event data, resulting in more stable performance across different motion scales. Therefore, in scenar-

Table 3. Ablation study on modules for 3D detection during blind time. DSGF: Dual Semantic-Geometric Filter. SDR: Semantic-Guided Depth Refinement. GSV: Geometric-Filtered Semantic Volume. OCRA: Object-Centric ROI Alignment. The fused voxel source is denoted as G or S, where G represents geometric voxel and S represents semantic voxel.

DSGF		3D Voxel Source	OCRA	mAP Easy	
SDR	GSV			3D	BEV
		G		12.92	20.78
		G+S		14.60	24.85
		G	✓	14.56	21.73
		G+S	✓	15.95	26.12
✓		G+S		15.85	27.78
	✓	G+S		17.08	26.53
✓	✓	G+S		19.12	29.64
✓	✓	G+S	✓	21.66	31.52

ios with high-speed driving or significant scene changes due to dynamic motion, our event-based 3D detection proves highly effective during blind time.

5. Ablation Study

Ablation Study on Modules. As shown in Table 3, we conduct an ablation study on the proposed modules. Starting from a baseline that performs 3D detection using only the geometric plane-sweep volume, we incrementally add the proposed modules to evaluate their impact on performance.

We report the easy mAP performance, which is the average value across the two classes, VEH and PED, measured under a motion scale of 1 and a time slice of 10. Compared to the baseline, simply adding semantic information results in sub-optimal performance, yielding only a 1.68 improvement in 3D detection. However, incorporating a dual semantic-geometric filter, which facilitates interaction between semantic and geometric features, leads to a significant performance gain of 6.2 in 3D detection. Additionally, the proposed object-centric ROI alignment consistently improves performance across all settings. When used along-

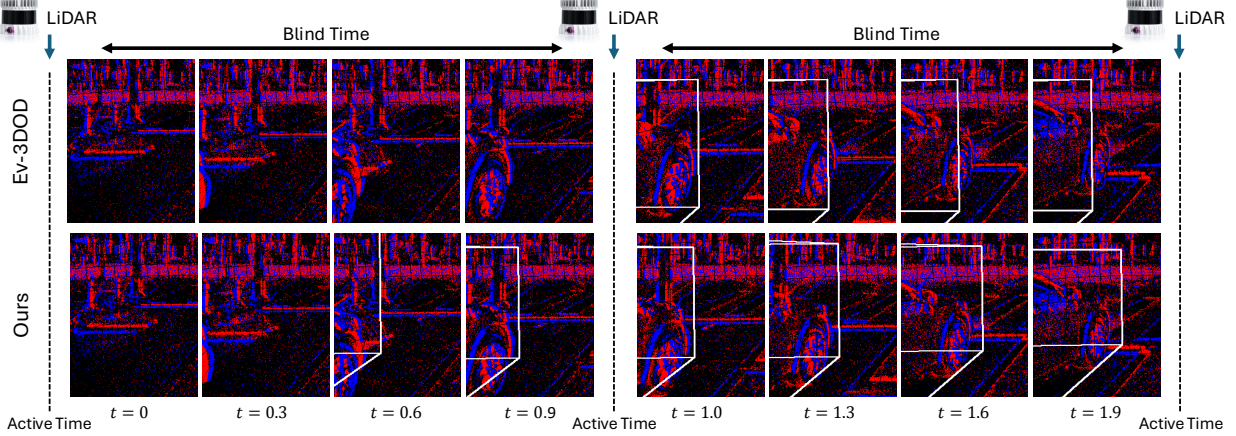


Figure 6. Comparison of 3D detection during blind time. Ev-3DOD detects new objects only at the active timestamps, $t = 0, 1, 2$, using LiDAR and RGB. In contrast, the proposed model can capture the emergence of new objects at arbitrary times.

Table 4. Performance of RGB fusion. Results of easy difficulty level with a time slice of 10.

Settings	Methods	AP_{3D}		AP_{BEV}	
		VEH	PED	VEH	PED
Motion $\times 1$	Ours (E)	23.47	19.86	40.13	22.91
	Ours (E+I)	25.23	21.50	46.21	29.14
Motion $\times 2$	Ours (E)	22.72	19.04	39.81	22.71
	Ours (E+I)	20.14	10.50	37.93	12.76

side a dual semantic-geometric filter, it further enhances semantic BEV features, resulting in a more significant performance boost.

RGB Fusion. Table 4 presents the results of fusing synchronous RGB information into our method. The stereo RGB features are extracted using a separate feature extractor and concatenated with the event features. This fusion provides improved performance under small motion scales, as the RGB input offers additional semantic guidance. However, under large motion, the performance significantly degrades due to misalignment between the synchronous RGB data and the actual object location. In contrast, our setup that relies solely on event data demonstrates robust performance regardless of scene dynamics.

Performance Degradation over Blind Time. Figure 7 shows the performance over time during blind time for our method and other methods [22, 50]. To highlight robustness in challenging scenarios, we use motion scale of 2. $t = 0$ refers to the most recent synchronized sensor input timestamp, while $t = 0.1 \sim 0.9$ represents the blind interval before the next input. The reason for the performance drop of other methods is that they rely on 3D information from synchronous sensors and struggle as the current scene diverges from recent active time ($t = 0$), making it challenging to estimate the present 3D box using past information. Thus, despite using event data, Ev-3DOD struggles to transfer past

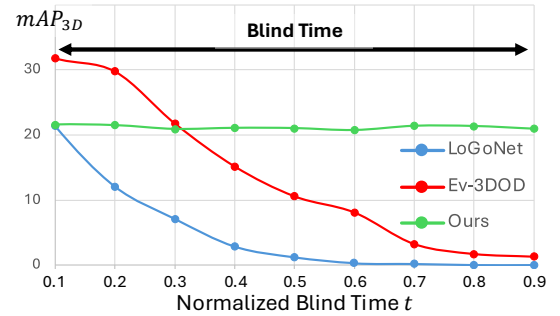


Figure 7. Performance comparison with other methods during blind time under the setting of motion scale 2 and time slice 10.

3D information to the present, causing its performance to resemble LoGoNet as motion increases over time. In contrast, our method asynchronously infers both geometric and semantic information for 3D detection, allowing it to operate independently of active time.

6. Conclusion

In this paper, we tackle 3D object detection using event stereo in a fully asynchronous setting for the first time. Unlike the previous continuous-time 3D object detection work that utilizes LiDAR, our approach does not rely on LiDAR, leading to lower performance compared to methods that fuse LiDAR and event data. However, by evaluating various motion scales and time slices, we demonstrate that our method is more adaptable and performs robustly in diverse and extreme conditions. Furthermore, we highlight the potential of event-based 3D perception in dynamic environments where event cameras are particularly beneficial, such as drone flights, high-speed driving, and robots. We hope this work inspires further research in this direction.

7. Acknowledgments.

This work was supported by the National Research Foundation of Korea(NRF) grant funded by the Korea government(MSIT) (NRF2022R1A2B5B03002636). This work was also supported by the Technology Innovation Program (1415187329,20024355, Development of autonomous driving connectivity technology based on sensor-infrastructure cooperation) funded By the Ministry of Trade, Industry & Energy(MOTIE, Korea).

References

- [1] Soikat Hasan Ahmed, Hae Woong Jang, SM Nadim Uddin, and Yong Ju Jung. Deep event stereo leveraged by event-to-image translation. In *Proceedings of the AAAI Conference on Artificial Intelligence*, pages 882–890, 2021. 2
- [2] Xuyang Bai, Zeyu Hu, Xinge Zhu, Qingqiu Huang, Yilun Chen, Hongbo Fu, and Chiew-Lan Tai. Transfusion: Robust lidar-camera fusion for 3d object detection with transformers. In *Proceedings of the IEEE/CVF conference on computer vision and pattern recognition*, pages 1090–1099, 2022. 2
- [3] Luca Bartolomei, Matteo Poggi, Andrea Conti, and Stefano Mattoccia. Lidar-event stereo fusion with hallucinations. In *European Conference on Computer Vision*, pages 125–145. Springer, 2024. 2
- [4] Anish Bhattacharya, Marco Cannici, Nishanth Rao, Yuezhan Tao, Vijay Kumar, Nikolai Matni, and Davide Scaramuzza. Monocular event-based vision for obstacle avoidance with a quadrotor. *arXiv preprint arXiv:2411.03303*, 2024. 6
- [5] Yin Bi, Aaron Chadha, Alhabib Abbas, Eirina Bourtsoulatz, and Yiannis Andreopoulos. Graph-based object classification for neuromorphic vision sensing. *2019 IEEE/CVF International Conference on Computer Vision (ICCV)*, pages 491–501, 2019. 2
- [6] Hu Cao, Zehua Zhang, Yan Xia, Xinyi Li, Jiahao Xia, Guang Chen, and Alois Knoll. Embracing events and frames with hierarchical feature refinement network for object detection. In *European Conference on Computer Vision*, pages 161–177. Springer, 2024. 2
- [7] Jia-Ren Chang and Yong-Sheng Chen. Pyramid stereo matching network. In *Proceedings of the IEEE Conference on Computer Vision and Pattern Recognition*, pages 5410–5418, 2018. 3
- [8] Liyan Chen, Weihang Wang, and Philippos Mordohai. Learning the distribution of errors in stereo matching for joint disparity and uncertainty estimation. In *Proceedings of the IEEE/CVF conference on computer vision and pattern recognition*, pages 17235–17244, 2023. 4
- [9] Xuanyao Chen, Tianyuan Zhang, Yue Wang, Yilun Wang, and Hang Zhao. Futr3d: A unified sensor fusion framework for 3d detection. *2023 IEEE/CVF Conference on Computer Vision and Pattern Recognition Workshops (CVPRW)*, pages 172–181, 2022. 2
- [10] Xihao Chen, Wenming Weng, Yueyi Zhang, and Zhiwei Xiong. Depth from asymmetric frame-event stereo: A divide-and-conquer approach. In *Proceedings of the IEEE/CVF Winter Conference on Applications of Computer Vision*, pages 3045–3054, 2024. 2
- [11] Yilun Chen, Shu Liu, Xiaoyong Shen, and Jiaya Jia. Dsgn: Deep stereo geometry network for 3d object detection. In *Proceedings of the IEEE/CVF conference on computer vision and pattern recognition*, pages 12536–12545, 2020. 2, 3, 5, 6, 7, 16, 17
- [12] Yilun Chen, Shijia Huang, Shu Liu, Bei Yu, and Jiaya Jia. Dsgn++: Exploiting visual-spatial relation for stereo-based 3d detectors. *IEEE Transactions on Pattern Analysis and Machine Intelligence*, 45(4):4416–4429, 2022. 2, 5
- [13] Yukang Chen, Yanwei Li, Xiangyu Zhang, Jian Sun, and Jiaya Jia. Focal sparse convolutional networks for 3d object detection. In *Proceedings of the IEEE/CVF Conference on Computer Vision and Pattern Recognition*, pages 5428–5437, 2022. 6, 7, 16
- [14] Yukang Chen, Jianhui Liu, Xiangyu Zhang, Xiaojuan Qi, and Jiaya Jia. Voxelnext: Fully sparse voxelnet for 3d object detection and tracking. In *Proceedings of the IEEE/CVF Conference on Computer Vision and Pattern Recognition*, pages 21674–21683, 2023. 6, 7, 16
- [15] Yi-Nan Chen, Hang Dai, and Yong Ding. Pseudo-stereo for monocular 3d object detection in autonomous driving. In *Proceedings of the IEEE/CVF conference on computer vision and pattern recognition*, pages 887–897, 2022. 2
- [16] Zehui Chen, Zhenyu Li, Shiquan Zhang, Liangji Fang, Qin-hong Jiang, and Feng Zhao. Deformable feature aggregation for dynamic multi-modal 3d object detection. In *European conference on computer vision*, pages 628–644. Springer, 2022. 2
- [17] Hoonhee Cho and Kuk-Jin Yoon. Event-image fusion stereo using cross-modality feature propagation. In *Proceedings of the AAAI Conference on Artificial Intelligence*, pages 454–462, 2022. 2
- [18] Hoonhee Cho and Kuk-Jin Yoon. Selection and cross similarity for event-image deep stereo. In *European Conference on Computer Vision*, pages 470–486. Springer, 2022. 2
- [19] Hoonhee Cho, Jaeseok Jeong, and Kuk-Jin Yoon. Eomvs: Event-based omnidirectional multi-view stereo. *IEEE Robotics and Automation Letters*, 6(4):6709–6716, 2021. 2
- [20] Hoonhee Cho, Jegyeong Cho, and Kuk-Jin Yoon. Learning adaptive dense event stereo from the image domain. In *Proceedings of the IEEE/CVF Conference on Computer Vision and Pattern Recognition*, pages 17797–17807, 2023. 14
- [21] Hoonhee Cho, Jae-Young Kang, and Kuk-Jin Yoon. Temporal event stereo via joint learning with stereoscopic flow. In *European Conference on Computer Vision*, pages 294–314. Springer, 2024. 2
- [22] Hoonhee Cho, Jae-Young Kang, Youngho Kim, and Kuk-Jin Yoon. Ev-3dod: Pushing the temporal boundaries of 3d object detection with event cameras. In *Proceedings of the IEEE/CVF Conference on Computer Vision and Pattern Recognition (CVPR)*, pages 27197–27210, 2025. 1, 2, 6, 7, 8, 14, 15, 16, 17
- [23] Jiajun Deng, Shaoshuai Shi, Peiwei Li, Wengang Zhou, Yanyong Zhang, and Houqiang Li. Voxel r-cnn: Towards

- high performance voxel-based 3d object detection. In *Proceedings of the AAAI conference on artificial intelligence*, pages 1201–1209, 2021. 5
- [24] Lue Fan, Ziqi Pang, Tianyuan Zhang, Yu-Xiong Wang, Hang Zhao, Feng Wang, Naiyan Wang, and Zhaoxiang Zhang. Embracing single stride 3d object detector with sparse transformer. In *Proceedings of the IEEE/CVF conference on computer vision and pattern recognition*, pages 8458–8468, 2022. 2
- [25] Tuo Feng, Ruijie Quan, Xiaohan Wang, Wenguan Wang, and Yi Yang. Interpretable3d: An ad-hoc interpretable classifier for 3d point clouds. In *Proceedings of the AAAI Conference on Artificial Intelligence*, pages 1761–1769, 2024. 2
- [26] Benedek Forrai, Takahiro Miki, Daniel Gehrig, Marco Hutter, and Davide Scaramuzza. Event-based agile object catching with a quadrupedal robot. In *2023 IEEE International Conference on Robotics and Automation (ICRA)*, pages 12177–12183. IEEE, 2023. 6
- [27] Guillermo Gallego, Tobi Delbrück, Garrick Orchard, Chiara Bartolozzi, Brian Taba, Andrea Censi, Stefan Leutenegger, Andrew J Davison, Jörg Conradt, Kostas Daniilidis, et al. Event-based vision: A survey. *IEEE transactions on pattern analysis and machine intelligence*, 44 (1):154–180, 2020. 1
- [28] Daniel Gehrig and Davide Scaramuzza. Pushing the limits of asynchronous graph-based object detection with event cameras. *ArXiv*, abs/2211.12324, 2022. 2
- [29] Daniel Gehrig and Davide Scaramuzza. Low-latency automotive vision with event cameras. *Nature*, 629:1034 – 1040, 2024. 2
- [30] Mathias Gehrig and Davide Scaramuzza. Recurrent vision transformers for object detection with event cameras. *2023 IEEE/CVF Conference on Computer Vision and Pattern Recognition (CVPR)*, pages 13884–13893, 2022. 2
- [31] Mathias Gehrig, Willem Aarents, Daniel Gehrig, and Davide Scaramuzza. Dsec: A stereo event camera dataset for driving scenarios. *IEEE Robotics and Automation Letters*, 6(3):4947–4954, 2021. 6
- [32] Andreas Geiger, Philip Lenz, and Raquel Urtasun. Are we ready for autonomous driving? the kitti vision benchmark suite. *2012 IEEE Conference on Computer Vision and Pattern Recognition*, pages 3354–3361, 2012. 6, 14
- [33] Tianrui Guan, Jun Wang, Shiyi Lan, Rohan Chandra, Zuxuan Wu, Larry Davis, and Dinesh Manocha. M3detr: Multi-representation, multi-scale, mutual-relation 3d object detection with transformers. In *Proceedings of the IEEE/CVF winter conference on applications of computer vision*, pages 772–782, 2022. 2
- [34] Xiaoyang Guo, Shaoshuai Shi, Xiaogang Wang, and Hongsheng Li. Liga-stereo: Learning lidar geometry aware representations for stereo-based 3d detector. In *Proceedings of the IEEE/CVF international conference on computer vision*, pages 3153–3163, 2021. 2, 3, 5, 6, 7, 16
- [35] Jesse Hagenaaers, Federico Paredes-Vallés, and Guido De Croon. Self-supervised learning of event-based optical flow with spiking neural networks. *Advances in Neural Information Processing Systems*, 34:7167–7179, 2021. 14
- [36] Ryuhei Hamaguchi, Yasutaka Furukawa, Masaki Onishi, and Ken Sakurada. Hierarchical neural memory network for low latency event processing. *2023 IEEE/CVF Conference on Computer Vision and Pattern Recognition (CVPR)*, pages 22867–22876, 2023. 2
- [37] Chenhang He, Hui Zeng, Jianqiang Huang, Xian-Sheng Hua, and Lei Zhang. Structure aware single-stage 3d object detection from point cloud. In *Proceedings of the IEEE/CVF conference on computer vision and pattern recognition*, pages 11873–11882, 2020. 2
- [38] Chenhang He, Ruihuang Li, Shuai Li, and Lei Zhang. Voxel set transformer: A set-to-set approach to 3d object detection from point clouds. In *Proceedings of the IEEE/CVF conference on computer vision and pattern recognition*, pages 8417–8427, 2022. 2
- [39] Jordan SK Hu, Tianshu Kuai, and Steven L Waslander. Point density-aware voxels for lidar 3d object detection. In *Proceedings of the IEEE/CVF conference on computer vision and pattern recognition*, pages 8469–8478, 2022. 2
- [40] Junjie Huang, Guan Huang, Zheng Zhu, Yun Ye, and Dalong Du. Bevdet: High-performance multi-camera 3d object detection in bird-eye-view. *arXiv preprint arXiv:2112.11790*, 2021. 2
- [41] Junjie Huang, Yun Ye, Zhujin Liang, Yi Shan, and Dalong Du. Detecting as labeling: Rethinking lidar-camera fusion in 3d object detection. In *European Conference on Computer Vision*, pages 439–455. Springer, 2025. 2
- [42] Yu Huang, Chenzhuang Du, Zihui Xue, Xuanyao Chen, Hang Zhao, and Longbo Huang. What makes multi-modal learning better than single (provably). *Advances in Neural Information Processing Systems*, 34:10944–10956, 2021. 2
- [43] Massimiliano Iacono, Stefan Weber, Arren J. Glover, and Chiara Bartolozzi. Towards event-driven object detection with off-the-shelf deep learning. *2018 IEEE/RSJ International Conference on Intelligent Robots and Systems (IROS)*, pages 1–9, 2018. 2
- [44] Yanqin Jiang, Li Zhang, Zhenwei Miao, Xiatian Zhu, Jin Gao, Weiming Hu, and Yu-Gang Jiang. Polarformer: Multi-camera 3d object detection with polar transformer. In *Proceedings of the AAAI conference on Artificial Intelligence*, pages 1042–1050, 2023. 2
- [45] Alex Kendall, Hayk Martirosyan, Saumitro Dasgupta, and Peter Henry. End-to-end learning of geometry and context for deep stereo regression. *2017 IEEE International Conference on Computer Vision (ICCV)*, pages 66–75, 2017. 5
- [46] Alex H Lang, Sourabh Vora, Holger Caesar, Lubing Zhou, Jiong Yang, and Oscar Beijbom. Pointpillars: Fast encoders for object detection from point clouds. In *Proceedings of the IEEE/CVF conference on computer vision and pattern recognition*, pages 12697–12705, 2019. 2
- [47] Dianze Li, Jianing Li, and Yonghong Tian. Sodformer: Streaming object detection with transformer using events and frames. *IEEE Transactions on Pattern Analysis and Machine Intelligence*, 45:14020–14037, 2023. 2
- [48] Jianing Li, Jia Li, Lin Zhu, Xijie Xiang, Tiejun Huang, and Yonghong Tian. Asynchronous spatio-temporal memory network for continuous event-based object detection. *IEEE Transactions on Image Processing*, 31:2975–2987, 2022. 2

- [49] Peiliang Li, Xiaozhi Chen, and Shaojie Shen. Stereo r-cnn based 3d object detection for autonomous driving. In *Proceedings of the IEEE/CVF Conference on Computer Vision and Pattern Recognition*, pages 7644–7652, 2019. [2](#)
- [50] Xin Li, Tao Ma, Yuenan Hou, Botian Shi, Yuchen Yang, Youquan Liu, Xingjiao Wu, Qin Chen, Yikang Li, Yu Qiao, et al. Logonet: Towards accurate 3d object detection with local-to-global cross-modal fusion. In *Proceedings of the IEEE/CVF Conference on Computer Vision and Pattern Recognition*, pages 17524–17534, 2023. [2](#), [6](#), [7](#), [8](#), [16](#), [17](#)
- [51] Xiaotian Li, Baojie Fan, Jiandong Tian, and Huijie Fan. Gafusion: Adaptive fusing lidar and camera with multiple guidance for 3d object detection. In *Proceedings of the IEEE/CVF Conference on Computer Vision and Pattern Recognition*, pages 21209–21218, 2024. [2](#)
- [52] Xiang Li, Junbo Yin, Wei Li, Chengzhong Xu, Ruigang Yang, and Jianbing Shen. Di-v2x: Learning domain-invariant representation for vehicle-infrastructure collaborative 3d object detection. In *Proceedings of the AAAI Conference on Artificial Intelligence*, pages 3208–3215, 2024. [2](#)
- [53] Yijin Li, Han Zhou, Bangbang Yang, Yexin Zhang, Zhaopeng Cui, Hujun Bao, and Guofeng Zhang. Graph-based asynchronous event processing for rapid object recognition. *2021 IEEE/CVF International Conference on Computer Vision (ICCV)*, pages 914–923, 2021. [2](#)
- [54] Yanwei Li, Yilun Chen, Xiaojuan Qi, Zeming Li, Jian Sun, and Jiaya Jia. Unifying voxel-based representation with transformer for 3d object detection. *Advances in Neural Information Processing Systems*, 35:18442–18455, 2022. [2](#)
- [55] Yanwei Li, Xiaojuan Qi, Yukang Chen, Liwei Wang, Zeming Li, Jian Sun, and Jiaya Jia. Voxel field fusion for 3d object detection. In *Proceedings of the IEEE/CVF Conference on Computer Vision and Pattern Recognition*, pages 1120–1129, 2022.
- [56] Yingwei Li, Adams Wei Yu, Tianjian Meng, Ben Caine, Jiquan Ngiam, Daiyi Peng, Junyang Shen, Yifeng Lu, Denny Zhou, Quoc V Le, et al. Deepfusion: Lidar-camera deep fusion for multi-modal 3d object detection. In *Proceedings of the IEEE/CVF conference on computer vision and pattern recognition*, pages 17182–17191, 2022. [2](#)
- [57] Yinhao Li, Zheng Ge, Guanyi Yu, Jinrong Yang, Zengran Wang, Yukang Shi, Jianjian Sun, and Zeming Li. Bevdepth: Acquisition of reliable depth for multi-view 3d object detection. In *Proceedings of the AAAI Conference on Artificial Intelligence*, pages 1477–1485, 2023. [2](#)
- [58] Tingting Liang, Hongwei Xie, Kaicheng Yu, Zhongyu Xia, Zhiwei Lin, Yongtao Wang, Tao Tang, Bing Wang, and Zhi Tang. Bevfusion: A simple and robust lidar-camera fusion framework. *Advances in Neural Information Processing Systems*, 35:10421–10434, 2022. [2](#)
- [59] Zhiwei Lin, Zhe Liu, Zhongyu Xia, Xinhao Wang, Yongtao Wang, Shengxiang Qi, Yang Dong, Nan Dong, Le Zhang, and Ce Zhu. Rcbvdet: Radar-camera fusion in bird’s eye view for 3d object detection. In *Proceedings of the IEEE/CVF Conference on Computer Vision and Pattern Recognition*, pages 14928–14937, 2024. [2](#)
- [60] Xianpeng Liu, Ce Zheng, Ming Qian, Nan Xue, Chen Chen, Zhebin Zhang, Chen Li, and Tianfu Wu. Multi-view attentive contextualization for multi-view 3d object detection. In *Proceedings of the IEEE/CVF Conference on Computer Vision and Pattern Recognition (CVPR)*, pages 16688–16698, 2024. [2](#)
- [61] Yuxuan Liu, Lujia Wang, and Ming Liu. Yolostereo3d: A step back to 2d for efficient stereo 3d detection. In *2021 IEEE international conference on Robotics and automation (ICRA)*, pages 13018–13024. IEEE, 2021. [2](#)
- [62] Yingfei Liu, Tiancai Wang, Xiangyu Zhang, and Jian Sun. Petr: Position embedding transformation for multi-view 3d object detection. In *European Conference on Computer Vision*, pages 531–548. Springer, 2022. [2](#)
- [63] Zhijian Liu, Haotian Tang, Alexander Amini, Xinyu Yang, Huizi Mao, Daniela L Rus, and Song Han. Bevfusion: Multi-task multi-sensor fusion with unified bird’s-eye view representation. In *2023 IEEE international conference on robotics and automation (ICRA)*, pages 2774–2781. IEEE, 2023. [2](#)
- [64] Ilya Loshchilov and Frank Hutter. Decoupled weight decay regularization. *arXiv preprint arXiv:1711.05101*, 2017. [14](#)
- [65] Hanyue Lou, Jinxiu Sherry Liang, Minggui Teng, Bin Fan, Yong Xu, and Boxin Shi. Zero-shot event-intensity asymmetric stereo via visual prompting from image domain. *Advances in Neural Information Processing Systems*, 37:13274–13301, 2025. [2](#)
- [66] Yan Lu, Xinzhu Ma, Lei Yang, Tianzhu Zhang, Yating Liu, Qi Chu, Junjie Yan, and Wanli Ouyang. Geometry uncertainty projection network for monocular 3d object detection. In *Proceedings of the IEEE/CVF International Conference on Computer Vision*, pages 3111–3121, 2021. [2](#)
- [67] Jiageng Mao, Yujing Xue, Minzhe Niu, Haoyue Bai, Jia-shi Feng, Xiaodan Liang, Hang Xu, and Chunjing Xu. Voxel transformer for 3d object detection. In *Proceedings of the IEEE/CVF international conference on computer vision*, pages 3164–3173, 2021. [2](#)
- [68] Zhenwei Miao, Jikai Chen, Hongyu Pan, Ruiwen Zhang, Kaixuan Liu, Peihan Hao, Jun Zhu, Yang Wang, and Xin Zhan. Pvgnet: A bottom-up one-stage 3d object detector with integrated multi-level features. In *Proceedings of the IEEE/CVF Conference on Computer Vision and Pattern Recognition*, pages 3279–3288, 2021. [2](#)
- [69] Mohammad Mostafavi, Kuk-Jin Yoon, and Jonghyun Choi. Event-intensity stereo: Estimating depth by the best of both worlds. In *Proceedings of the IEEE/CVF International Conference on Computer Vision*, pages 4258–4267, 2021. [2](#)
- [70] Yeongwoo Nam, Mohammad Mostafavi, Kuk-Jin Yoon, and Jonghyun Choi. Stereo depth from events cameras: Concentrate and focus on the future. In *Proceedings of the IEEE/CVF Conference on Computer Vision and Pattern Recognition*, 2022. [2](#)
- [71] Su Pang, Daniel Morris, and Hayder Radha. Clocs: Camera-lidar object candidates fusion for 3d object detection. In *2020 IEEE/RSJ International Conference on Intelligent Robots and Systems (IROS)*, pages 10386–10393. IEEE, 2020. [2](#)

- [72] Yan Peng, Yueyi Zhang, Peilin Xiao, Xiaoyan Sun, and Feng Wu. Better and faster: Adaptive event conversion for event-based object detection. In *AAAI Conference on Artificial Intelligence*, 2023. 2
- [73] Yansong Peng, Yueyi Zhang, Zhiwei Xiong, Xiaoyan Sun, and Feng Wu. Get: Group event transformer for event-based vision. *2023 IEEE/CVF International Conference on Computer Vision (ICCV)*, pages 6015–6025, 2023. 2
- [74] Yansong Peng, Hebei Li, Yueyi Zhang, Xiaoyan Sun, and Feng Wu. Scene adaptive sparse transformer for event-based object detection. *2024 IEEE/CVF Conference on Computer Vision and Pattern Recognition (CVPR)*, pages 16794–16804, 2024. 2
- [75] Etienne Perot, Pierre de Tournemire, Davide Oscar Nitti, Jonathan Masci, and Amos Sironi. Learning to detect objects with a 1 megapixel event camera. *ArXiv*, abs/2009.13436, 2020. 2
- [76] AJ Piergiovanni, Vincent Casser, Michael S Ryoo, and Anelia Angelova. 4d-net for learned multi-modal alignment. In *Proceedings of the IEEE/CVF International Conference on Computer Vision*, pages 15435–15445, 2021. 2
- [77] Matteo Poggi, Seungryong Kim, Fabio Tosi, Sunok Kim, Filippo Aleotti, Dongbo Min, Kwanghoon Sohn, and Stefano Mattoccia. On the confidence of stereo matching in a deep-learning era: a quantitative evaluation. *IEEE transactions on pattern analysis and machine intelligence*, 44(9): 5293–5313, 2021. 4
- [78] Aditya Prakash, Kashyap Chitta, and Andreas Geiger. Multi-modal fusion transformer for end-to-end autonomous driving. In *Proceedings of the IEEE/CVF conference on computer vision and pattern recognition*, pages 7077–7087, 2021. 2
- [79] Simon Schaefer, Daniel Gehrig, and Davide Scaramuzza. Aegnn: Asynchronous event-based graph neural networks. In *IEEE Conference on Computer Vision and Pattern Recognition*, 2022. 2
- [80] Amit Shaked and Lior Wolf. Improved stereo matching with constant highway networks and reflective confidence learning. In *Proceedings of the IEEE conference on computer vision and pattern recognition*, pages 4641–4650, 2017. 4
- [81] Hualian Sheng, Sijia Cai, Yuan Liu, Bing Deng, Jianqiang Huang, Xian-Sheng Hua, and Min-Jian Zhao. Improving 3d object detection with channel-wise transformer. In *Proceedings of the IEEE/CVF international conference on computer vision*, pages 2743–2752, 2021. 2
- [82] Shaoshuai Shi, Xiaogang Wang, and Hongsheng Li. Pointcnn: 3d object proposal generation and detection from point cloud. In *Proceedings of the IEEE/CVF conference on computer vision and pattern recognition*, pages 770–779, 2019. 2
- [83] Shaoshuai Shi, Chaoxu Guo, Li Jiang, Zhe Wang, Jianping Shi, Xiaogang Wang, and Hongsheng Li. Pv-rcnn: Point-voxel feature set abstraction for 3d object detection. In *Proceedings of the IEEE/CVF conference on computer vision and pattern recognition*, pages 10529–10538, 2020. 2
- [84] Weijing Shi and Raj Rajkumar. Point-gnn: Graph neural network for 3d object detection in a point cloud. In *Proceedings of the IEEE/CVF conference on computer vision and pattern recognition*, pages 1711–1719, 2020. 2
- [85] Shintaro Shiba, Yoshimitsu Aoki, and Guillermo Gallego. Secrets of event-based optical flow. In *European Conference on Computer Vision*, pages 628–645. Springer, 2022. 14
- [86] Ziyang Song, Lei Yang, Shaoqing Xu, Lin Liu, Dongyang Xu, Caiyan Jia, Feiyang Jia, and Li Wang. Graphbev: Towards robust bev feature alignment for multi-modal 3d object detection. *arXiv preprint arXiv:2403.11848*, 2024. 2
- [87] Jiaming Sun, Linghao Chen, Yiming Xie, Siyu Zhang, Qin-hong Jiang, Xiaowei Zhou, and Hujun Bao. Disp r-cnn: Stereo 3d object detection via shape prior guided instance disparity estimation. In *Proceedings of the IEEE/CVF conference on computer vision and pattern recognition*, pages 10548–10557, 2020. 2
- [88] Stepan Tulyakov, Daniel Gehrig, Stamatios Georgoulis, Julius Erbach, Mathias Gehrig, Yuanyou Li, and Davide Scaramuzza. Time lens: Event-based video frame interpolation. In *Proceedings of the IEEE/CVF conference on computer vision and pattern recognition*, pages 16155–16164, 2021. 14
- [89] Sourabh Vora, Alex H Lang, Bassam Helou, and Oscar Beijbom. Pointpainting: Sequential fusion for 3d object detection. In *Proceedings of the IEEE/CVF conference on computer vision and pattern recognition*, pages 4604–4612, 2020. 2
- [90] Dongsheng Wang, Xu Jia, Yang Zhang, Xinyu Zhang, Yaoyuan Wang, Ziyang Zhang, D. Wang, and Huchuan Lu. Dual memory aggregation network for event-based object detection with learnable representation. In *AAAI Conference on Artificial Intelligence*, 2023. 2
- [91] Wenjie Wang, Yehao Lu, Guangcong Zheng, Shuigen Zhan, Xiaoqing Ye, Zichang Tan, Jingdong Wang, Gaoang Wang, and Xi Li. Bevspread: Spread voxel pooling for bird’s-eye-view representation in vision-based roadside 3d object detection. In *Proceedings of the IEEE/CVF Conference on Computer Vision and Pattern Recognition*, pages 14718–14727, 2024. 2
- [92] Yue Wang, Vitor Campagnolo Guizilini, Tianyuan Zhang, Yilun Wang, Hang Zhao, and Justin Solomon. Detr3d: 3d object detection from multi-view images via 3d-to-2d queries. In *Conference on Robot Learning*, pages 180–191. PMLR, 2022. 2
- [93] Yan Wang, Junbo Yin, Wei Li, Pascal Frossard, Ruigang Yang, and Jianbing Shen. Ssd3d: Semi-supervised domain adaptation for 3d object detection from point cloud. In *Proceedings of the AAAI Conference on Artificial Intelligence*, pages 2707–2715, 2023. 2
- [94] Yichen Xie, Chenfeng Xu, Marie-Julie Rakotosaona, Patrick Rim, Federico Tombari, Kurt Keutzer, Masayoshi Tomizuka, and Wei Zhan. Sparsefusion: Fusing multi-modal sparse representations for multi-sensor 3d object detection. *2023 IEEE/CVF International Conference on Computer Vision (ICCV)*, pages 17545–17556, 2023. 2
- [95] Gangwei Xu, Junda Cheng, Peng Guo, and Xin Yang. Attention concatenation volume for accurate and efficient

- stereo matching. In *Proceedings of the IEEE/CVF Conference on Computer Vision and Pattern Recognition*, pages 12981–12990, 2022. [4](#)
- [96] Jianyun Xu, Zhenwei Miao, Da Zhang, Hongyu Pan, Kaixuan Liu, Peihan Hao, Jun Zhu, Zhengyang Sun, Hongmin Li, and Xin Zhan. Int: Towards infinite-frames 3d detection with an efficient framework. In *European Conference on Computer Vision*, pages 193–209. Springer, 2022. [2](#)
- [97] Shaoqing Xu, Dingfu Zhou, Jin Fang, Junbo Yin, Zhou Bin, and Liangjun Zhang. Fusionpainting: Multimodal fusion with adaptive attention for 3d object detection. In *2021 IEEE International Intelligent Transportation Systems Conference (ITSC)*, pages 3047–3054. IEEE, 2021. [2](#)
- [98] Zetong Yang, Yanan Sun, Shu Liu, Xiaoyong Shen, and Jiaya Jia. Std: Sparse-to-dense 3d object detector for point cloud. In *Proceedings of the IEEE/CVF international conference on computer vision*, pages 1951–1960, 2019. [2](#)
- [99] Zetong Yang, Yanan Sun, Shu Liu, and Jiaya Jia. 3dssd: Point-based 3d single stage object detector. In *Proceedings of the IEEE/CVF conference on computer vision and pattern recognition*, pages 11040–11048, 2020. [2](#)
- [100] Zeyu Yang, Jiaqi Chen, Zhenwei Miao, Wei Li, Xiatian Zhu, and Li Zhang. Deepinteraction: 3d object detection via modality interaction. *Advances in Neural Information Processing Systems*, 35:1992–2005, 2022. [2](#)
- [101] Man Yao, Huanhuan Gao, Guangshe Zhao, Dingheng Wang, Yihan Lin, Zhao-Xu Yang, and Guoqi Li. Temporal-wise attention spiking neural networks for event streams classification. *2021 IEEE/CVF International Conference on Computer Vision (ICCV)*, pages 10201–10210, 2021. [2](#)
- [102] Junbo Yin, Dingfu Zhou, Liangjun Zhang, Jin Fang, Cheng-Zhong Xu, Jianbing Shen, and Wenguan Wang. Proposal-contrast: Unsupervised pre-training for lidar-based 3d object detection. In *European conference on computer vision*, pages 17–33. Springer, 2022. [2](#)
- [103] Junbo Yin, Jianbing Shen, Runnan Chen, Wei Li, Ruigang Yang, Pascal Frossard, and Wenguan Wang. Is-fusion: Instance-scene collaborative fusion for multimodal 3d object detection. In *Proceedings of the IEEE/CVF Conference on Computer Vision and Pattern Recognition*, pages 14905–14915, 2024. [2](#)
- [104] Gang Zhang, Junnan Chen, Guohuan Gao, Jianmin Li, Si Liu, and Xiaolin Hu. Safdnet: A simple and effective network for fully sparse 3d object detection. In *Proceedings of the IEEE/CVF Conference on Computer Vision and Pattern Recognition (CVPR)*, pages 14477–14486, 2024. [2](#)
- [105] Gang Zhang, Chen Junnan, Guohuan Gao, Jianmin Li, and Xiaolin Hu. Hednet: A hierarchical encoder-decoder network for 3d object detection in point clouds. *Advances in Neural Information Processing Systems*, 36, 2024. [6](#), [7](#), [16](#)
- [106] Kaixuan Zhang, Kaiwei Che, Jianguo Zhang, Jie Cheng, Ziyang Zhang, Qinghai Guo, and Luziwei Leng. Discrete time convolution for fast event-based stereo. In *Proceedings of the IEEE/CVF Conference on Computer Vision and Pattern Recognition*, pages 8676–8686, 2022. [2](#)
- [107] Fengan Zhao, Qianang Zhou, and Junlin Xiong. Edge-guided fusion and motion augmentation for event-image stereo. In *European Conference on Computer Vision*, pages 190–205. Springer, 2024. [2](#)
- [108] Dingfu Zhou, Jin Fang, Xibin Song, Liu Liu, Junbo Yin, Yuchao Dai, Hongdong Li, and Ruigang Yang. Joint 3d instance segmentation and object detection for autonomous driving. In *Proceedings of the IEEE/CVF Conference on Computer Vision and Pattern Recognition*, pages 1839–1849, 2020. [2](#)
- [109] Alex Zihao Zhu, Yibo Chen, and Kostas Daniilidis. Real-time time synchronized event-based stereo. In *Proceedings of the European Conference on Computer Vision (ECCV)*, pages 433–447, 2018. [2](#)
- [110] Alex Zihao Zhu, Liangzhe Yuan, Kenneth Chaney, and Kostas Daniilidis. Ev-flownet: Self-supervised optical flow estimation for event-based cameras. *arXiv preprint arXiv:1802.06898*, 2018. [14](#)
- [111] Alex Zihao Zhu, Liangzhe Yuan, Kenneth Chaney, and Kostas Daniilidis. Unsupervised event-based learning of optical flow, depth, and egomotion. In *Proceedings of the IEEE/CVF Conference on Computer Vision and Pattern Recognition*, pages 989–997, 2019. [3](#), [14](#)
- [112] Dongqing Zou, Feng Shi, Weiheng Liu, Jia Li, Qiang Wang, Paul-KJ Park, Chang-Woo Shi, Yohan J Roh, and Hyun-suk Eric Ryu. Robust dense depth map estimation from sparse dvs stereos. In *British Mach. Vis. Conf.(BMVC)*, 2017. [2](#)
- [113] Nikola Zubic, Daniel Gehrig, Mathias Gehrig, and Davide Scaramuzza. From chaos comes order: Ordering event representations for object recognition and detection. *2023 IEEE/CVF International Conference on Computer Vision (ICCV)*, pages 12800–12810, 2023. [2](#)

Unleashing the Temporal Potential of Stereo Event Cameras for Continuous-Time 3D Object Detection

Supplementary Material

1. Details of Motion Scale and Time Slice

Figure 1 provides details of our experimental setup. To ensure a fair comparison with previous works, Sec. 4.3 of the main paper adopts the same evaluation protocol. DSEC-3DOD provides a fixed-frame-rate sensor at 10 FPS and blind time annotations at 100 FPS. Provided LiDAR and RGB data are fully utilized, and each blind time is evaluated with 10 ground truth annotations.

The evaluation setup of Ev-3DOD [22] allows for assessing detection performance during blind time. However, due to the limited motion in DSEC data and its fixed time intervals, model performance can only be evaluated at restricted points in time. To enable evaluation under asynchronous and diverse temporal conditions, we define motion scale and time slice as key evaluation setup parameters.

Motion scale is a parameter that controls scene motion by adjusting the length of the blind time. This is achieved by skipping consecutive frames of LiDAR and RGB data, thereby modifying the amount of motion. Events are accumulated over the blind time and normalized in the temporal domain. Motion scale control [20, 35, 85, 88, 110, 111], which accumulates data over a longer period to represent large motion, is a well-established method widely used in other works for evaluating performance under large motion conditions. Therefore, following previous work, we also adopted motion scale control to represent dynamic and long-range motion.

Time slice controls the evaluation interval within the blind time. Each blind time is evaluated at multiple points determined by the time slice. This parameter introduces variations in the distribution of event data, making it a challenging factor for assessing the temporal flexibility of event-based methods.

We define the baseline experimental setup with a motion scale of 1 and a time slice of 10. Evaluations were conducted using various experimental parameters within the constraints of the given fixed-frame-rate sensor and available annotations. To ensure a fair evaluation, we assessed detection performance using only the model trained on the baseline setup.

2. Implementation Details

Training Details. Training was conducted on two NVIDIA TITAN RTX GPUs for 60 epochs with a batch size of 2. The AdamW optimizer [64] was employed with a learning rate set to 0.001.

Depth Refinement. To perform actual refinement, we computed a finer probability by considering neighboring probabilities. Thus, the practical implementation of Eq. (6) in the main paper incorporates neighboring pixels as follows:

$$S(u, v) = \langle F_L^{sem}(u, v), F_R^{sem}(u - \frac{fL}{D_{init}^m(u, v)}, v) \rangle, \quad (1)$$

We use the $m = 1, 2, 3, 4, 5$ for neighboring sampling.

Event Grid size and Voxel Size. Following previous works [22], we use the bin size of event voxel grid as 5. 3D geometric voxel and 3D semantic voxel in Sec. 3.3 have range of $[-30.4m, 30.4m]$ in X axis, $[-1.0m, 3.0m]$ in Y axis, and $[2.0m, 56.9m]$ for Z axis. Voxel size is set to $(0.2m, 0.2m, 0.2m)$.

ROI Pooling for Alignment In Sec. 3.5 of the main paper, the ROI P_G estimated by the global detector is divided into a $k \times k$ voxel grid, for $k = 3$. The semantic BEV features are pooled for each grid, and all grid features are aggregated to estimate the local offset.

Anchor Size As mentioned in the main paper, we use anchors with fixed size, height and orientation for each (x, z) coordinate in the 3D voxel space. The fixed anchor sizes are determined by computing the class-wise box statistics from the training set. Anchors for vehicle class and pedestrian class are as follows:

$$\begin{aligned} A_{veh} &= (x, 0.47, z, 1.79, 1.86, 4.28, \{0, \frac{\pi}{2}\}) \\ A_{ped} &= (x, 0.6, z, 1.73, 0.6, 0.8, \{0, \frac{\pi}{2}\}) \end{aligned} \quad (2)$$

3. Effectiveness of Semantic-guided Depth Refinement

Following the KITTI stereo metric [32], we measure a depth estimation accuracy if depth error is below a specified outlier threshold. Table 1 compares performance across different outlier thresholds, highlighting the impact of semantic-guided depth refinement (SDR). The results show that SDR consistently enhances accuracy across all thresholds. Moreover, the depth refinement module improves not only the final detection performance but also the overall depth estimation quality.

4. Visualization on Semantic and Geometric Features

Semantic and geometric event features serve distinct roles, and the model utilizes them collaboratively to enhance both

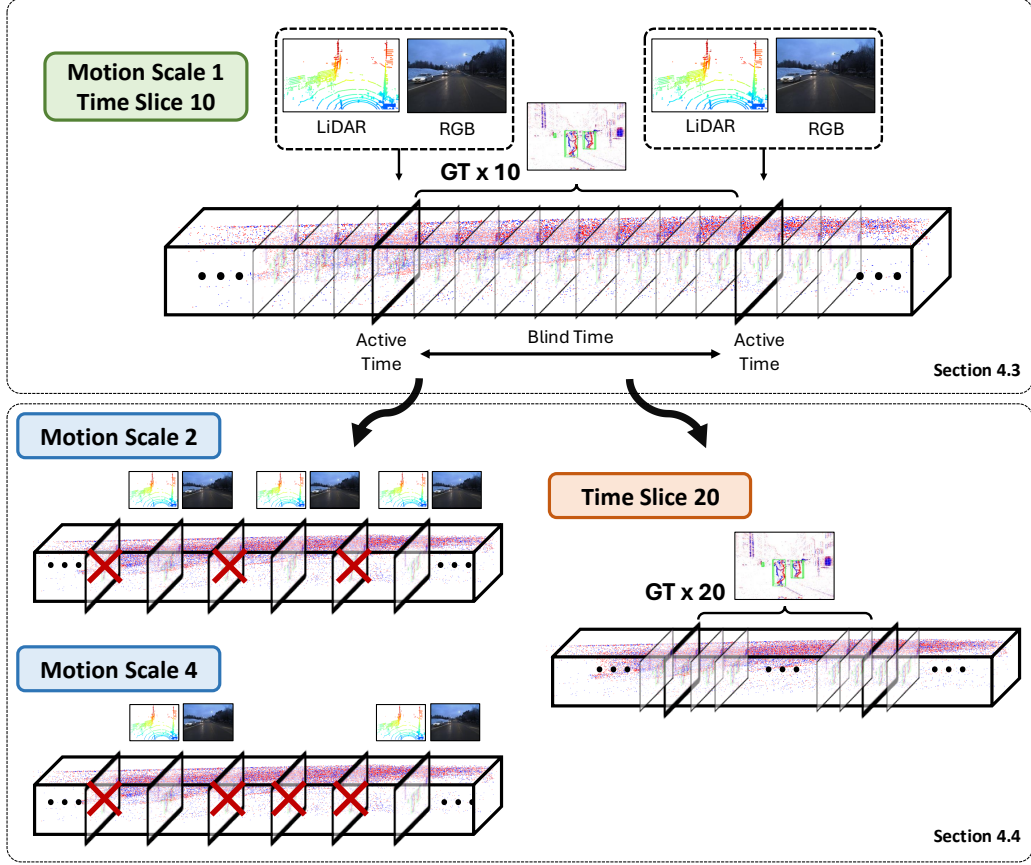


Figure 1. Visualization of the motion scale and time slice used in the experimental setup. The upper part of the figure represents the baseline setup following Ev-3DOD [22], with a motion scale of 1 and a time slice of 10. The lower part illustrates the setup adopted to evaluate the model under large motion and diverse event inputs.

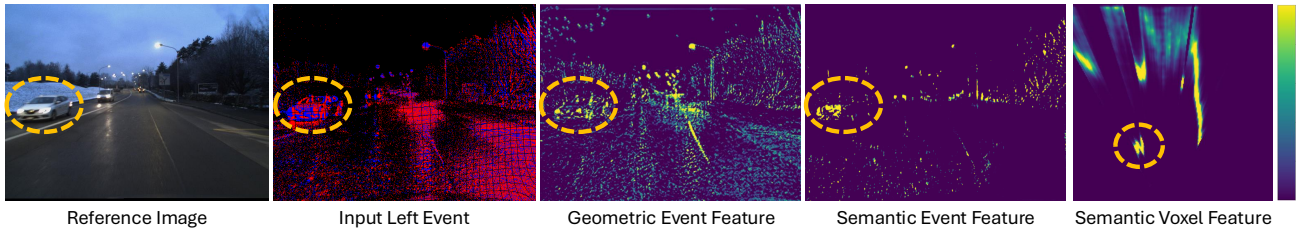


Figure 2. Example of input event, geometric feature, enhanced semantic feature, and semantic BEV feature. Feature values are normalized to $[0, 1]$ for visualization.

Table 1. Effectiveness of semantic-guided depth refinement. SDR: Semantic-Guided Depth Refinement.

Outlier Threshold	$> 1.6m$	$> 0.8m$	$> 0.4m$	$> 0.2m$
w/o SDR	0.236	0.382	0.549	0.715
w/ SDR (Ours)	0.219	0.361	0.529	0.696

geometric and semantic information. To provide insights into the characteristics of these features, we present visualizations of the extracted representations. Geometric features highlight complex structures that aid in stereo matching, whereas semantic features exhibit strong attention to

target objects. By leveraging such object-centric information, ROI alignment is achieved, enabling fine-grained box regression.

5. Additional Results

Quantitative Results. Table 2 presents the quantitative results of DSEC-3DOD at the moderate difficulty level, evaluated under various motion scales and time slices. Compared to our method, other approaches exhibit more significant performance degradation under large motions and longer

Table 2. Performance evaluation across various motion scales and time slices, presenting results for the moderate difficulty level. Each entry corresponds to 3D / BEV detection results. VEH and PED represent vehicle and pedestrian, respectively.

Motion Scale	Time Slice	Class	LiDAR		LIDAR+RGB		LiDAR+RGB+Event	RGB Stereo		Event Stereo
			VoxelNeXt [14]	HEDNet [105]	Focals Conv [13]	LoGoNet [50]	Ev-3DOD [22]	DSGN [11]	LIGA [34]	Ours
×2	×10	VEH	4.28 / 12.58	5.24 / 12.06	5.60 / 11.66	4.93 / 12.21	<u>13.52</u> / <u>26.56</u>	7.02 / 16.03	5.52 / 11.93	19.31 / 32.47
		PED	2.43 / 3.13	1.70 / 2.48	2.14 / 2.81	1.71 / 2.62	<u>4.91</u> / <u>8.57</u>	1.27 / 1.88	1.75 / 2.29	12.56 / 13.99
	×20	VEH	3.80 / 11.54	4.67 / 11.08	5.56 / 10.79	4.60 / 11.23	<u>14.50</u> / <u>27.93</u>	6.75 / 14.36	4.77 / 11.08	19.62 / 33.03
		PED	<u>2.31</u> / 2.48	1.49 / 2.18	1.52 / 2.15	1.44 / 2.24	1.62 / <u>3.19</u>	1.26 / 1.77	1.42 / 2.12	12.93 / 14.34
×4	×10	VEH	2.03 / 5.22	2.85 / 4.78	2.73 / 3.96	1.88 / 4.37	<u>5.59</u> / <u>10.50</u>	3.08 / 6.27	1.82 / 4.50	16.42 / 29.01
		PED	0.91 / 1.18	0.91 / 0.91	0.91 / 1.06	0.91 / 0.91	<u>2.31</u> / <u>3.37</u>	0.41 / 0.49	0.91 / 1.05	10.61 / 13.86
	×20	VEH	1.59 / 4.29	2.27 / 4.09	2.73 / 3.55	1.88 / 3.99	<u>5.60</u> / <u>10.26</u>	3.06 / 5.62	1.36 / 3.87	19.31 / 32.47
		PED	<u>0.91</u> / 0.91	<u>0.91</u> / 0.91	<u>0.91</u> / 0.91	0.45 / 0.91	<u>0.91</u> / <u>1.31</u>	0.34 / 0.46	0.45 / 0.69	12.93 / 14.34

blind times, as they heavily rely on synchronized sensors (e.g., RGB and LiDAR).

Qualitative Results.

We provide additional qualitative results for the motion scale 2 and time slice 10 setup. The results demonstrate that conventional sensor-based methods suffer from significant detection errors due to large motion. Furthermore, compared to Fig. 5 in the main paper, where the motion scale is set to 10, Ev-3DOD exhibits a substantial performance drop despite utilizing event data, as it remains heavily dependent on LiDAR. In contrast, our fully asynchronous model seamlessly adapts to large motion, ensuring robust detection.

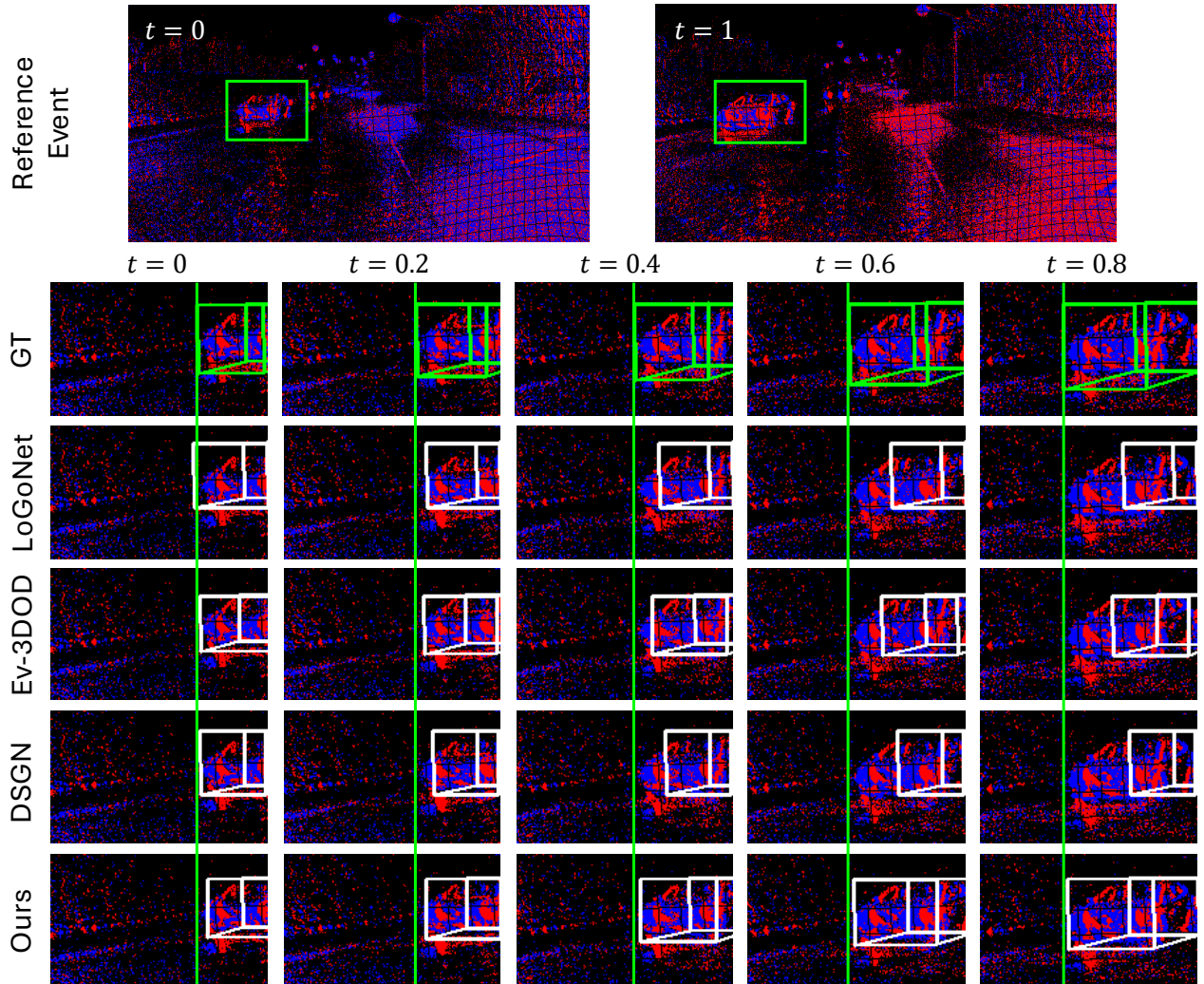


Figure 3. Comparison of 3D detection during blind time. The motion scale and time slice are set to 2 and 10, respectively. Green vertical lines across the image were added to compare the box’s relative position. Fixed-frame-rate sensor-based methods (*i.e.*, LoGoNet [50] and DSGN [11]) fail to predict objects during the blind time. Ev-3DOD [22] leverages monocular event data to propagate detection through blind time, but its performance deteriorates under large movements. The proposed method operates in a fully asynchronous manner, consistently producing stable results regardless of the blind time.